Electronic Supplementary Material (ESI) for Chemical Communications.

(Para)magnetic hybrid nanocarriers for dual MRI detection and treatment of solid tumours.

Cátia Vieira Rocha,[a] Milene Costa da Silva, [a] Manuel Bañobre-Lopez [a] and Juan Gallo [a]*

Supplementary information

Index

S1 - Synthesis Methods

Hydrophobic nanoparticles of magnetite (Fe_3O_4@OA) were prepared by coprecipitation method adapted from [1]. Briefly, 9.2 g of iron(II) chloride tetrahydrate and 15 g of iron(III) chloride hexahydrate were dissolved in 250 mL of mili-Q water and stirred for 10 min at 50 °C. After 10 min, 30 mL of ammonium hydroxide, NH4OH (12 mol/L), were added starting this way the coprecipitation that resulted in a dark precipitate of Fe_3O_4. Then 2.5 mL of oleic acid (OA) were added and the mixture was heated at 80 °C for 1 h. The excess of NH4OH and OA was removed by magnetic separation of Fe_3O_4@OA with the use of a magnet, followed by the decantation of the supernatant and the redispersion of the solid in fresh solvent. The washing procedure was repeated five times with milli-Q water and four times with hexane. Finally, the Fe_3O_4@OA NPs were dried, dispersed in chloroform and stored at 4º C [2].

Hydrophobic manganese oxide (MnO@OA) nanoparticles were prepared according to [3]. For the preparation, 0.5 g of potassium permanganate ($KMnO_4$) were dissolved in 250 mL of Milli-Q water and left stirring for about 30 mins. A total of 5 mL of OA were added and the sample was left stirring, at room temperature, for 24 h. The next day there was a brown 'solid' floating on a colourless solution, this solution was decanted and the solid washed twice with mili-Q water. After this, ethanol (EtOH) was added to remove any possible residue reactants. At this point the solid was resuspended in the solvent, transferred to falcon tubes and centrifuged for 5 min at 8500 rpm. The supernatant was once more discarded and the pellet resuspended in hexane, resulting in a dark-brown solution that was stored in the fridge until further use.

A modified melt-emulsification method was used for the preparation of HNCs. Initially, 200 mg of carnauba wax were mixed in a glass vial with a colloidal $CHCl_3$ solution of MNPs (Fe_3O_4 10% and MnO 20%, % with respect to the mass of wax), 0.25 mL of a chloroform solution of DiO (1 mg/mL), added only in final formulations, and Dox. This mixture was then placed in the Digital Sonifier. At this point, 4.5 mL of Milli-Q water and 0.5 mL of a water solution of Tween® 80 (50 mg/ml) were added to the vial and the sample was ultrasonicated with a 3 mm tip, for 2 min, at 25% power, at 20 second working intervals, while being simultaneously heated with a heat gun. Immediately after the sonication, the sample was immersed in ice to solidify the lipid NPs. Once cold, the formulation was centrifuged for 10 min, at 3000 RPM to remove big wax aggregates, the supernatant was stored in a glass vial and the pellet was discarded.

S2 - General Information

Initially, to study the encapsulation efficiency (EE) of Dox into the SLNs, an aliquot was taken from the sample right after its synthesis, while it was immersed in ice. Then, this aliquot was extracted with chloroform. After a few minutes the non-encapsulated dox was extracted to the chloroform that was then pippetted into a HPLC vial and its dox concentration measured by HPLC. Prior to the EE measurements, a dox calibration curve was determined by HPLC using a

gradient of water: acetonitrile (from 100% to 25:75%) and an Aeris 1.7 µm peptide XB-C18 column. Fluorescent detection (460 nm excitation, 560 nm emission) was used for the identification of dox peak. This calibration curve was used to calculate the dox EE, using the following equation:

$$EE\% = \frac{[\text{encapsulated drug}]}{[\text{total drug}]} \times 100$$

For the characterization of the HNCs particles different equipment were used. To measure the average size, PI and the zeta potential of the HNCs a Dynamic Light Scattering – Zeta potential, SZ-100Z equipment from Horiba Scientific with nanometric resolution (from 0.3 nm to 8 µm) was used. For all the measurements an electrode cell was used. For all the measurements 1 mL of sample was used, with a dilution of 1:100, since it was the ratio at which the lowest PI values could be obtained.

A TEM, JEOL JEM-2100-HT (Cryo & Tomography), with an accelerating voltage between 80 kV and 200 kV and a resolution of 0.24 nm was used to analyze the morphology and composition of the synthetized MNPs and HNCs. Its major use was for the HNCs, to verify if the MNPs were efficiently encapsulated. This instrument is equipped with a high brightness LaB_6 (lanthanum hexaboride) electron gun and a fast-readout OneView 4k x 4k CCD camera.

For the infra-red spectra acquisition a FT-IR - Vertex 80v from Bruker was used. The operation mode used in this work was the MIR-ATR mode. The detector used was a very sensitive MCT (Mercury-Cadmium-Telluride) detector, cooled with liquid nitrogen.

ICP-AES was used to determine the concentration of each MNP in the HNCs. To establish a calibration cure for each element, standard solutions were prepared for iron (ranged from 0 to 10 ppm) and for manganese (ranged from 0 to 0.5 ppm). To analyse the concentration of iron and manganese the emission wavelengths used were 235 nm and 257 nm, respectively.

An X-Ray Diffraction System, X'Pert PRO MRD from PANalytical with a copper X-ray tube (CuKα) in a Bragg Brentano configuration was used to identify the samples crystallographic structure.

The acquisition of fluorescence spectra was made with a Compact Spectrofluorometer, FluoroMax-4 from Horiba Scientific. This technique was used to analyse the samples of HNCs containing Dox, to confirm the presence of the drug, since it is a fluorescent drug with an emission peak around 590 nm. The emission spectra of DiO, a fluorescent dye with an emission at around 506 nm, was also recorded. The spectra were acquired from 500 to 700 nm, using 5 nm entrance and exit slits, with λ_{ex} of 480 nm. For the spectra acquisition the samples were highly diluted, and a four opening disposable cell was used.

A TGA/DSC 1, 1100 SF, STARe system from Mettler Toledo was used to obtain the percentage of inorganic content present inside the HNCs. The analysis was performed under a nitrogen atmosphere. The method used consisted in a temperature increase from 25 to 900 ºC at 10ºC/min, with an approximately 30 min stop at 120 ºC to assure that all the water had evaporated.

To magnetically characterise HNCs and magnetite NPs a SQUID-VSM, MPMS magnetometer from Quantum Design was used. This equipment combines the SQUID technology with a vibrating sample measurement, also used in the VSM equipment. For the magnetization measurements the samples were submitted to a magnetic field of 100 Oe at 5 K and 300 K. To magnetically characterize MnO NPs a VSM 3473-70 electromagnet with a coil gap of 127 mm, from GMW was used. For these measurements a magnetic field of $\pm$ 2 T was applied.

T_1 and T_2 maps were studied in this work. The evaluated formulations were: Mn-HNCs, Fe-HNCS and mHNCS-Dox. All the samples were measured at a magnetic field of 3.0 T and room temperature. MR imaging was performed at room temperature in a 3.0 T horizontal bore MR Solutions Benchtop MRI system equipped with 48 G cm−1 actively shielded gradients. To image the samples, a 56 mm diameter quadrature birdcage coil was used in transmit/ receive mode. Samples (from 0 to 133 uM Fe and from 0 to 25 uM Mn) were placed on a custom-printed PLA

sample holder (300 µL) which was then placed in the center of the scanner. Longitudinal relaxation times were measured from T_1 maps acquired using MPRAGE sequences (TI = 11 values (0.275, 0.3, 0.35, 0.45, 0.65, 1.05, 1.85, 3.45, 6.65, 12.45, 26.25 s), TE = 5 ms, TR = 10 s), while transversal relaxation times were measured from T_2 maps acquired through MEMS sequences (TE = 10 values (0.015, 0.03, 0.045, 0.06, 0.075, 0.09, 0.105, 0.12, 0.135, 0.15, 0.165, 0.18, 0.195, 0.21, 0.225 s), TR = 1400 ms). T_1 and T_2 maps were reconstructed using ImageJ software (http://imagej.nih.gov/ij), particularly the "MRI analysis calculator" plugin by Karl Schmidt. The final relaxivities (r_1/r_2) were calculated from the slope of the linear fit of the relaxation rates versus the Mn concentration for T_1 and the Fe concentration for T_2.All MR images were acquired with an image matrix 256 × 252, FOV 60 × 60 mm with 3 slices with a slice thickness of 1 mm and no slice gap for T_2 maps, and 1 slice with 2.0 mm thickness for T_1 maps.

To understand if both magnetic nanoparticles were able to produce contrast, T_1 and T_2 maps for HNCs containing each of the MNPs in question (Fe-HNCs, Mn-HNCs) were also acquired as a preliminary study. The relaxation times can be easily interpreted resorting to the calibration bar present in each map. First, the T_2 map of the HNCs containing only 5% of iron (Fe-HNCs) was acquired to evaluate the CA efficiency of the encapsulated SPIONs at different concentrations. Fig. S3a shows the results obtained for the transverse relaxation weighted map of these particles. The Fe-HNCs achieved a good T_2 enhancement even at low concentrations and start to show some signal saturation around 60-75 µM under the conditions tested. The sample presents shorter relaxation times at higher concentrations, demonstrating its efficiency as a T_2 CA. The r_2 value in water for the Fe-HNCs was 183 mM^{-1} s^{-1}, which is higher than the FDA approved superparamagnetic iron oxide CAs Feridex® (r_2= 93 mM^{-1} s^{-1}) and Resovist® (r_2= 143 mM^{-1} s^{-1}) [4]. Then, the T_1 map of the HNCs containing manganese oxide (Mn-HNCs) was acquired to evaluate the contrast efficacy of the encapsulated MNPs at different concentrations. Fig. S3b shows the longitudinal relaxation weighted map measured for these particles, at increasingly higher concentrations. The T_1-weighted images show a great difference in contrast between the lower and higher concentrations, demonstrating the good performance of the particles as T_1 contrast enhancers. The r_1 value in water for the sample of Mn-HNCs was 1.25 mM^{-1} s^{-1}, which is close to the manganese-based T_1 CA Teslascan® (r_1= 1.5 mM^{-1} s^{-1}), approved by the FDA [4].

MH technique was used in various steps of this work, one of them being the characterisation of the heating efficiency of the final HNCs, through the calculation of the specific absorption rate (SAR) of the mHNCs-Dox. To this effect a MH equipment DM1 from nanoScale Biomagnetics was used. The frequency was set to 869.0 KHz and the intensity of the magnetic field was set to 20 mT. The sample was subjected to an AMF for 1 h straight, inducing a temperature increase that was recorded in a graph of temperature variation as a function of time. The SAR value was calculated using the following equation (1):

$$SAR = \frac{\mathrm{cdT}}{m_{NP} dt}$$

where c is the heat capacity, and dT is the temperature increment in a certain time (dt), and m_{NP} is the mass of the NP in question per mL of water.

For the *in vitro* studies Hs578T triple negative breast carcinoma cells were used. The cells were maintained in Dulbecco's modified Eagle's medium (DMEM) supplemented with 10 % fetal bovine serum (FBS) and 1 % Penicillin-Streptomycin and cultured in a 37 °C incubator with humidified atmosphere of 5% CO_2.

To evaluate if the MNPs were toxic by themselves, cytotoxicity studies with Hs578T cells were performed. The cells were seeded onto 96-well plates (2000 cells per well) and left to adhere for 24 h. Afterwards, cells were incubated with the HNCs at different concentrations respective to the metal ion (Fe, Mn, Fe+Mn). Cell viability was assessed at 48 h using AquaBluer as an indicator of viable cells according to the manufacturer's recommendations.

To study the internalization of the NPs in cells, Hs578T cells were seeded in a 24 well plate onto coverslips at a density of 10^5 cells/well and left to adhere for 24 h. Cells were then incubated with mHNCS-Dox at a concentration of 5 μg/mL of Dox (corresponding [Fe]=0,163 μg/mL and [Mn]=0,031 μg/mL - total ion concentration of 0,194μg/ml) for 4 h. Thereafter cells were washed twice with PBS (pH = 7.4) and fixed/permeabilized in ice cold methanol for 5 minutes at room temperature. Then, cells were washed with PBS and incubated with a mouse monoclonal anti-α-tubulin antibody for 1 hour at 37°C, followed by a washing step with PBS and incubation with an anti-mouse secondary antibody conjugated with AlexaFluor 647 for 1 hour at 37°C. Afterwards, cells were washed with PBS and incubated with DAPI for 5 minutes at room temperature, washed again in PBS and mounted onto a microscope slide using the Shandon Immu-mount mounting media. Cells were visualized under a scanning confocal microscope LSM780 on an inverted Axio Observer microscope from Zeiss, with the following lasers: 405 nm (DAPI); 488 nm (DiO); 561 nm (Dox); 633 nm (α-tubulin – AlexaFluor 647).

For the confocal experiments after MH, Hs578T cells were seeded in a cell culture dish (35/10 mm) and left to adhere for 24h. Cells were incubated with mHNCs-Dox at a final concentration of 10 μg/mL of Dox. Cells were placed in a MH applicator (+MH) for one hour under an electromagnetic field (H=20 mT, f=224,53 kHz) or left without MH (Control). Afterwards, cells were placed at 37 °C in an incubator with humidified atmosphere of 5 % CO_2 for 1 h hour and visualized under a scanning confocal microscope on an inverted Axio Observer LSM780 microscope from Zeiss, with the 561 nm laser (Dox). In addition, cells were stained with Hoechst 33342 nucleic acid stain and visualized with the lasers 405 nm (Hoechst) and 561 nm (Dox). The quantification of the overall signal intensity was done using ImageJ software.

For the MH studies, Hs578T cells were seeded in a cell culture dish (35/10 mm) with 4 compartments at a density of 10^4 cells/well and left to adhere for 24h. Cells were incubated with the samples at a final concentration of 2 μg/mL of Dox (or corresponding amount of Fe_3O_4, 0,044 μg/mL, in the case of mHNCS). The cell culture dish was placed in a MH applicator for one hour under an electromagnetic field (H=20 mT; f=224,53 kHz). Cells were then placed at 37 °C in an incubator with humidified atmosphere of 5 % CO_2 for 48 hours and viability was measured using AquaBluer as an indicator of viable cells.

Results from *in vitro* experiments are expressed as mean $\pm$ standard error of the mean. Comparisons between 3 or more independent groups and between groups with two independent variables were performed with 1- or 2-way ANOVA, respectively, and for tests with two groups a non-parametric t test was performed. All tests were followed by the Bonferroni posttest. $p<0,05$ was considered significant.

S3 – Characterization

The hydrodynamic size obtained for these particles from dynamic light scattering was about 170$\pm$14 nm with a polydispersity index (PI) of 0.24$\pm$0.06. The zeta potential was positive (29$\pm$1 mV), following the incorporation of Dox, since control particles without Dox presented a negative zeta potential value (-48.1$\pm$0.6 mV). Figure 1b (main article) shows the TEM micrographs of the synthetized mHNCs-Dox. From the images the incorporation of the NPs into the mHNCs-Dox is clear, and can also be confirmed by the EDXS analysis (Fig. S1c). Fe_3O_4 NPs appear as hypointense dots (yellow arrows), while MnO NPs are visible as elongated structures (blue arrows). Interestingly, both MNPs are simultaneously encapsulated into the mHNCs without segregation. The encapsulation efficiency of Dox was quantified to be over 99% due to its lipophilic nature and thus good affinity for the lipid matrix (S2).

S3.1- Optical characterization

The optical properties of our nanoparticles were studied by fluorescence spectroscopy in a Fluoromax. Fig. S1a shows the fluorescence spectra for the mHNCs-Dox, at an excitation wavelength of 480 nm for the Dox and 489 nm for the fluorescent dye, DiO. Since both the excitation wavelengths are very close, their spectra are identical showing three different peaks. The first and less intense peak, at 506 nm corresponds to the fluorescence emission of DiO[5]. The

next two peaks, at 557 and 590 nm, correspond to the fluorescence emission of Dox, which matches the typical fluorescence spectrum of this drug [6,7]. The observed optical behavior confirms the presence of Dox and DiO in the NPs, and the intensity of the peaks is in accordance with the quantities of each compound in the formulation.

S3.2- Thermogravimetric analysis

The TGA curve for our formulation presents two steps of weight loss and it is shown in Fig. S1b. The first and biggest step of weight loss, ①, represents the degradation of the organic components of the HNCs. As stated before, this step of weight loss from 250 to 500 ºC corresponds to the degradation of the surfactant Tween 80, Carnauba wax, OA and Doxorubicin [8–12]. The second step of weight loss above 750 ºC, ②, may be due to the degradation of magnetite[13]. The inorganic content of HNCS@Fe_3O_4-MnO-Dox is approximately 47 %.

S3.3- Fourier Transform Infra-red Spectroscopy

The FTIR graph displays all the important spectra to characterize the final HNCS formulation. The band at 560 cm^{-1} in the Fe_3O_4@OA spectrum corresponds to the symmetric Fe-O bonds stretching in the crystalline lattice of magnetite, and can also be found in the spectrum of the mHNCs-Dox[13]. Around 1407 cm^{-1} a band appears that corresponds to the CH_3 umbrella mode of the OA, thus the presence of this group is also noticed in the MnO@OA spectrum[13]. In this last spectrum the peak around 425 cm^{-1} can be assigned to be the Mn-O stretching mode, which does not appear in any other spectra probably due to the small concentration of MnO in the HNCs[14]. Next in the MnO@OA spectrum two peaks at 1457 cm^{-1} and 1710 cm^{-1} appear and are attributed to the asymmetric (-COO-) stretching mode and to the stretching vibration of (C=O) group, respectively. These functional groups are both present in the OA molecule, and the two peaks are also present in the wax and Tween 80 resulting in a more the CH_2 skeleton vibration, that can also be noticed in Tween 80, and consequently in the HNCs spectra[15]. The more distinct peak in the Tween 80 spectra is at 1100 cm^{-1} and corresponds to the stretching vibration of (C-O) groups, heavily present in Tween 80 chemical structure[15]. Consequently, these groups also appear very pronounced in both HNCS formulations. In the Tween 80 and HNCs spectra, there is also a broad peak at around 3500 cm^{-1} that corresponds to the stretching vibration of (O-H) groups[15]. In the final nanoparticle formulation, containing both MNPs and Dox, a new band appears at 1610 cm^{-1}. This band corresponds to the bending vibration mode of (N-H) groups, present in Dox[15]. In general, the results obtained by FT-IR are in accordance with what was expected, allowing the visualization of each component of the HNCs, in the final formulation.

S3.3- X-ray diffraction

The X-ray diffraction pattern of the mHNCs-Dox (Fig. 1d) unequivocally confirms the presence of both types of MNPs. XRD spectra are dominated by two peaks at low 2y values originated by the wax. Then, diffraction peaks with 2y values of 30.1, 35.5, 43.1, 53.5, 57 and 62.6 degrees correspond to the known Bragg reflections of magnetite (COD: 96-90095838), which are indexed as (220), (311), (400), (422), (511) and (440)[16] while diffraction peaks at 35.2 and 40.9 degrees come from MnO (COD: 96-101-0394), and are indexed as (111) and (200)[16].

S3.4- Magnetic Hyperthermia

Hs578T cells treated with mHNCs-Dox and submitted to MH for 1 h were observed in the confocal microscope in order to evaluate the effect of MH in the internalization of nanoparticles and drug release in cells. Fig.7A shows cells treated only with mHNCs-Dox, being that the observed red fluorescence corresponds to Dox. We can observe that in the cells submitted to 1 h of MH (with MH), the drug is not only internalized in the cell cytoplasm, but is also exerting its

action on the cell nucleus. The nucleus form and outlines are pronounced in cells submitted to MH, while in control cells (without MH) the Dox distribution is restricted to the cytoplasm. In Fig.7B a nuclear staining was used to better identify the nucleus position and confirm the presence of Dox inside the nucleus. In control cells it is possible to observe the presence of Dox mainly in the cytoplasm, while in cells submitted to MH Dox is already accumulating in the nucleus. Overall, we can conclude that MH acts as a triggering stimuli for the controlled release of Dox from the mHNCs.

Table S1 - List of abbreviations used throughout the manuscript and corresponding description.

Abbreviation	**Description**
HNCs	Hybrid nanocomposites
HNCs-Dox	Hybrid nanocomposites encapsulating Dox
Mn-HNCs	Hybrid nanocomposites encapsulating only MnO
Fe-HNCs	Hybrid nanocomposites encapsulating only Fe_3O_4
mHNCs	Hybrid nanocomposites encapsulating both MnO and Fe_3O_4
mHNCs-Dox	Hybrid nanocomposites encapsulating MnO, Fe_3O_4 and Dox

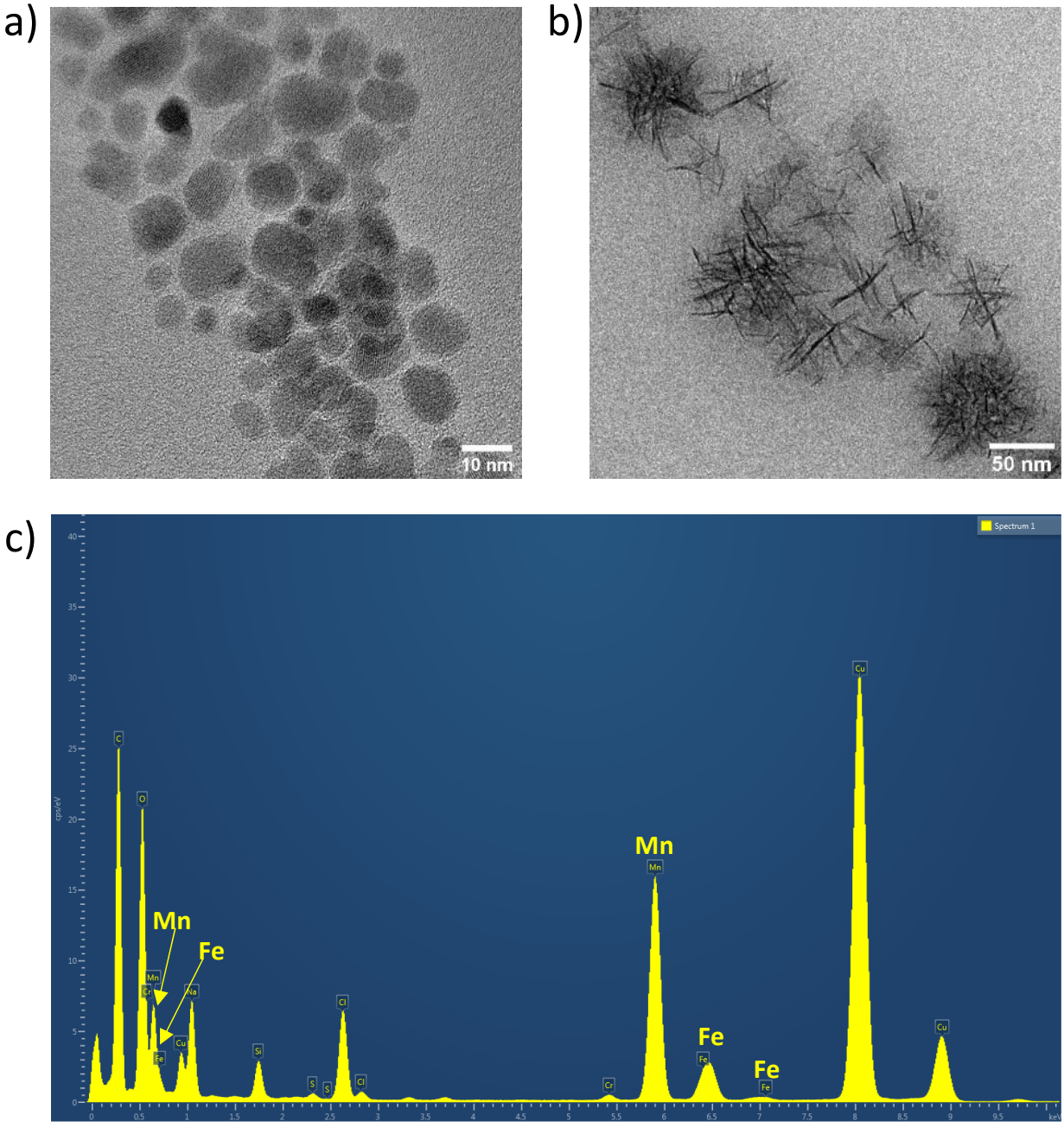

Fig. S1 - TEM micrographs of Fe3O4@OA NPs (a) and MnO@OA NPs (b) and EDX spectrum of mHNCs-Dox (c).

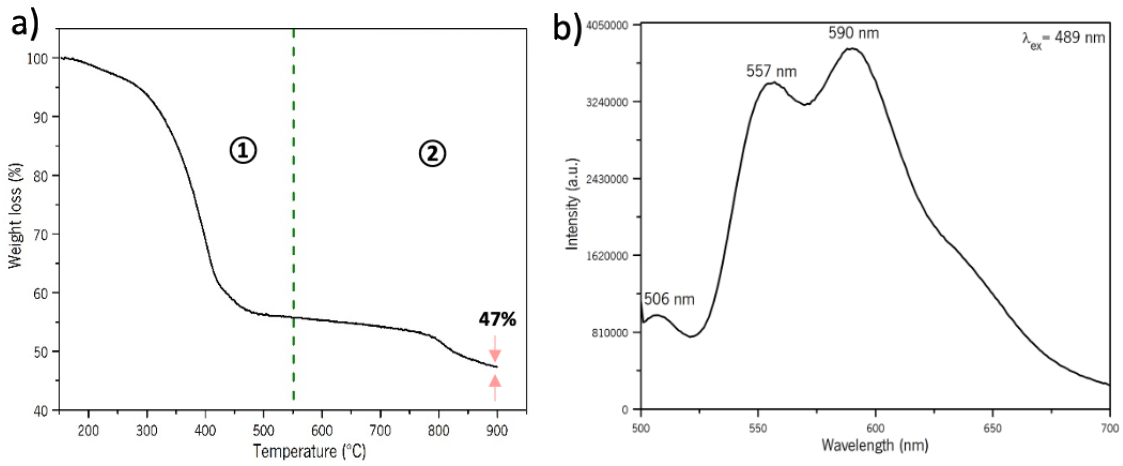

Fig. S2- Thermogravimetric profile in N_2 atmosphere (a) and fluorescence spectra at an excitation wavelength of 489 nm.

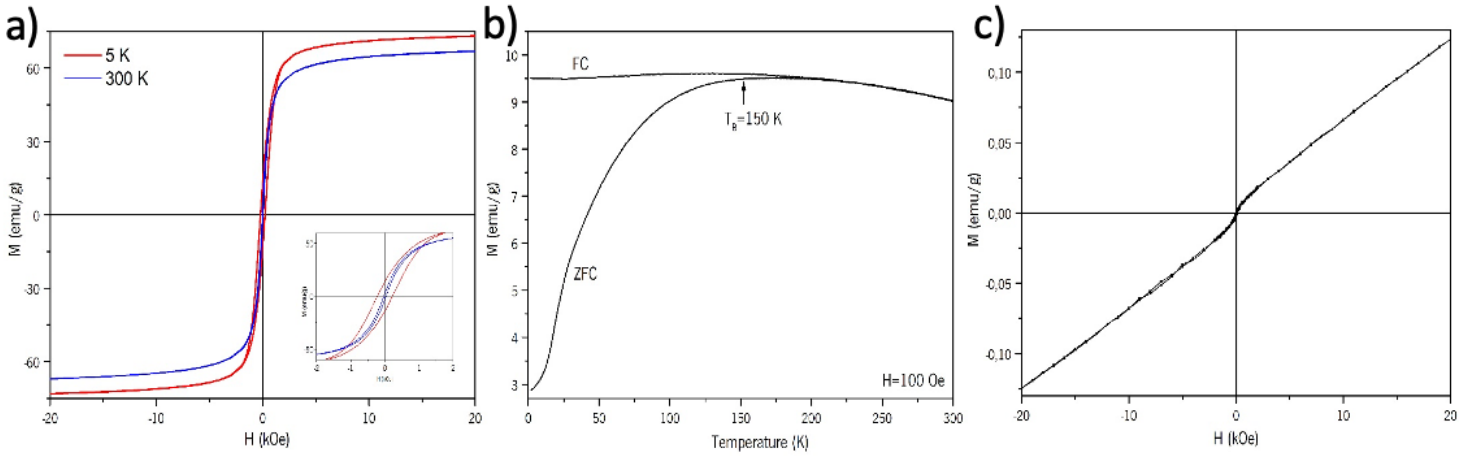

Fig. S3 – (a) Field-dependent magnetization curves of OA-capped magnetite NPs at 5 and 300 K. The inset is a close-up of both curves; (b) ZFC-FC magnetization curves under a magnetic field of 100 Oe and (c) VSM graph of MnO NPs.

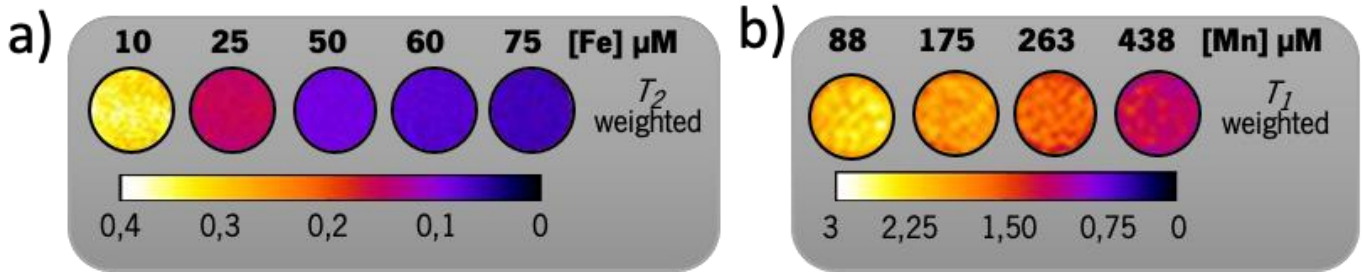

Fig. S4 - MRI T_2 map of Fe-HNCs (a) and MRI T_1 map of Mn-HNCs (b).

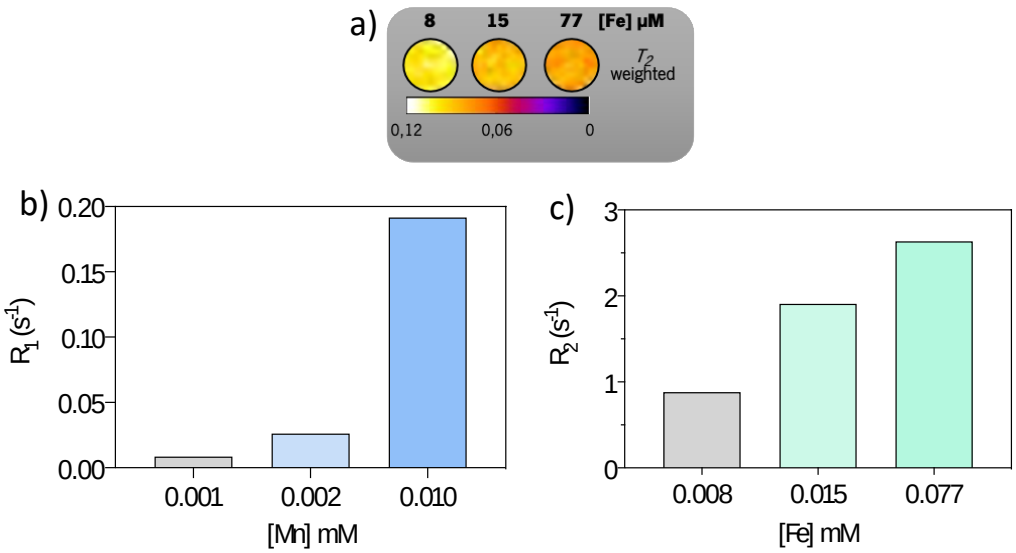

Fig. S5 – (a) MRI parametric T2 map of Hs578T cells treated with mHNCs-Dox; Longitudinal (b) and transverse (c) relaxation rates for different concentrations of MNPs.

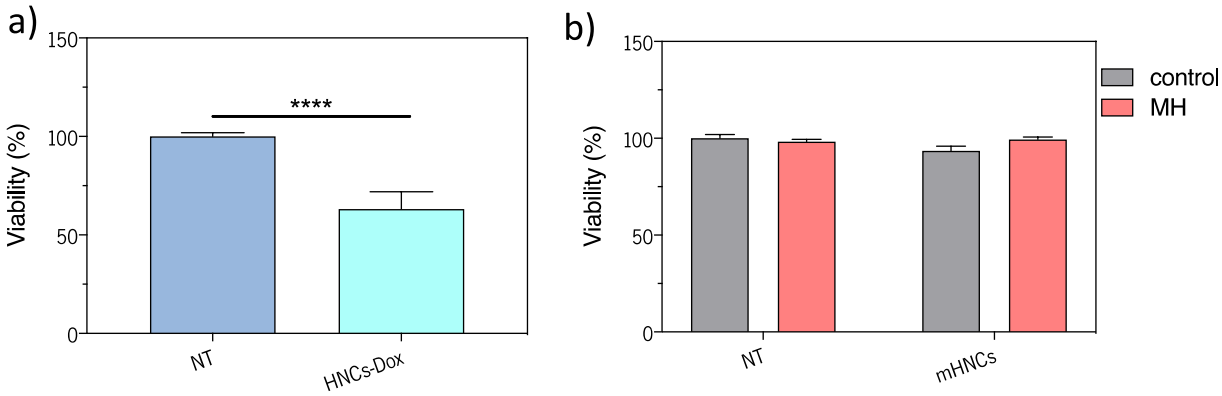

*Fig. S6 - Hs578T cell viability after treatment with HNCs-Dox (a) and after treatment with mHNCs, with (pink) and without MH (grey) (b). The data represent the mean value SEM of triplicate cultures in two different experiments. *p<0.05; **p<0.01;***p<0.001;****p<0.0001.*

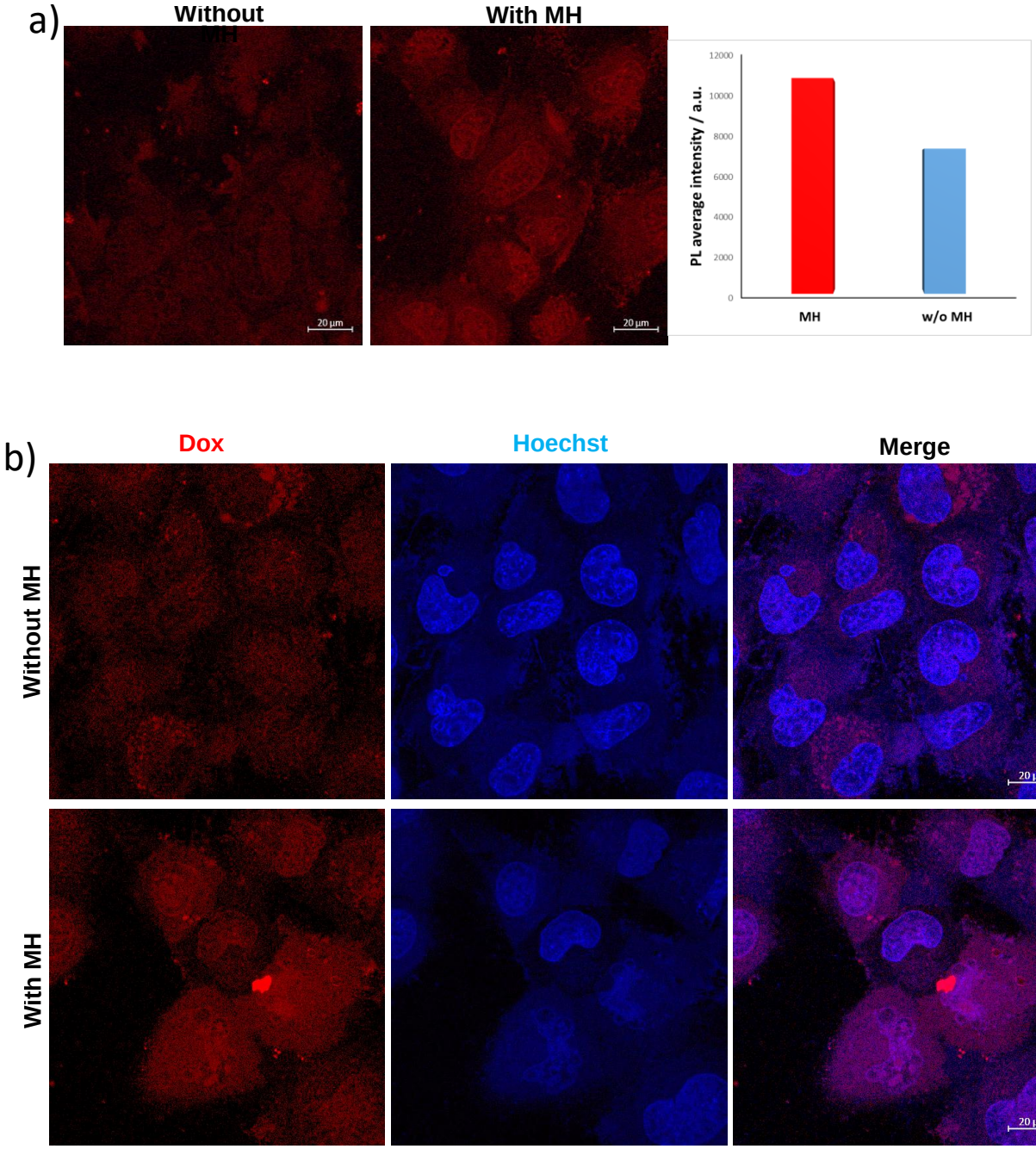

Fig. S7- (a) Dox distribution in Hs578T cells treated with mHNCs-Dox without MH (left) and with MH for 1 h (right); quantification of the average fluorescent intensity in both situations. (b) Dox distribution and nuclear staining in Hs578T cells incubated with mHNCs-Dox without MH and submitted to MH for 1 h. Pictures are representative of 2 independent experiments.

Bibliographic references

1 N. V Jadhav, A. I. Prasad, A. Kumar, R. Mishra, S. Dhara, K. R. Babu, C. L. Prajapat, N. L. Misra, R. S. Ningthoujam, B. N. Pandey and R. K. Vatsa, *Colloids Surf. B. Biointerfaces*, 2013, **108**, 68–158.

2 R. R. de Almeida, J. Gallo, A. C. C. da Silva, A. K. O. da Silva, O. D. L. Pessoa, T. G. Araújo, L. K. A. M. Leal, P. B. A. Fechine, M. Bañobre-López and N. M. P. S. Ricardo, *J. Braz. Chem. Soc.*, 2017, **28**, 1547–1556.

3 H. Chen, J. He, C. Zhang and H. He, *J. Phys. Chem. C*, 2007, **111**, 18033–18038.

4 M. Rohrer, H. Bauer, J. Mintorovitch, M. Requardt and H. J. Weinmann, *Invest. Radiol.*, 2005, **40**, 715–724.

5 ThermoFisher, Fluorescence SpectraViewer - PT, https://www.thermofisher.com/pt/en/home/life-science/cell-analysis/labeling-chemistry/fluorescence-spectraviewer.html?SID=srch-svtool&UID=275lip, (accessed 29 September 2019).

6 K. K. Karukstis, E. H. Z. Thompson, J. A. Whiles and R. J. Rosenfeld, *Biophys. Chem.*, 1998, **73**, 249–263.

7 P. Kumar and S. Agnihotri, *Biochem. Physiol. Open Access*, 2016, **5**, 1–6.

8 R. S. K. Kishore, A. Pappenberger, I. B. Dauphin, A. Ross, B. Buergi, A. Staempfli and H. C. Mahler, *J. Pharm. Sci.*, 2011, **100**, 721–731.

9 J. Milanovic, V. Manojlovic, S. Levic, N. Rajic, V. Nedovic and B. Bugarski, *Sensors*, 2010, **10**, 901–912.

10 J. Luo, L. Zhao, Y. Yang, G. Song, Y. Liu, L. Chen and G. Tang, *Sol. Energy Mater. Sol. Cells*, 2016, **147**, 144–149.

11 A. Lanz-Landázuri, A. Martínez De Ilarduya, M. García-Alvarez and S. Muñoz-Guerra, *React. Funct. Polym.*, 2014, **81**, 45–53.

12 K. Petcharoen and A. Sirivat, *Mater. Sci. Eng. B Solid-State Mater. Adv. Technol.*, 2012, **177**, 421–427.

13 K. Yang, H. Peng, Y. Wen and N. Li, *Appl. Surf. Sci.*, 2010, **256**, 3093–3097.

14 M. Balamurugan, G. Venkatesan, S. Ramachandran and S. Saravanan, in *Synthesis and Fabrication of Nanomaterials*, eds. V. Rajendran, P. Paramasivam and K. E. Geckeler, Bloomsbury Publishing India, 2015, pp. 311–314.

15 E. Pretsch, J. Seibl and W. Simon, in *Tablas para la determinación estructural por métodos espectroscópicos*, eds. A. Fernandéz and R. Álvarez, Springer - Verlag Ibérica, 3rd edn., 1998, pp. 16–50.

16 D. Chateigner, X. Chen, M. Ciriotti, R. T. Downs, S. Gražulis, W. Kaminsky, A. Le Bail, L. Lutterotti, Y. Matsushita, A. Merkys, P. Moeck, P. Murray-Rust, M. Q. Olozábal, H. Rajan and A. F. T. Yokochi, Crystallography Open Database, http://www.crystallography.net/cod/, (accessed 18 September 2019).